Alpha modulation of spiking activity across multiple brain regions in mice performing a tactile selective detection task

Craig Kelley, Cody Slater, Marc Sorrentino, Dillon Noone, Jocelyn Hung, Paul Sajda, and Qi Wang

Department of Biomedical Engineering, Columbia University, New York, NY 10027

Correspondence should be addressed to: qi.wang@columbia.edu

Keywords: Alpha oscillation, tactile selective detection task, whiskers, prefrontal cortex, primary somatosensory cortex, striatum

Abstract

A number of cognitive and sensory processes are characterized by strong relationships between the timing of neuronal spiking activity and the phase of ongoing local field potential oscillations. The coupling of neuronal spiking activity in neocortex to the phase of alpha oscillations (8-12 Hz) has been well studied in monkeys but remains largely unexplored in other mammals. How these relationships differ between brain areas and cell types, and how they relate to somatosensory signal detection and decision making, are not well understood. We used high density microelectrode arrays to chronically record neural activity from somatosensory cortex, prefrontal cortex, striatum, and amygdala in mice performing a head-fixed whisker-based selective detection task. We observed strong spontaneous alpha phase modulation of single neuron spiking activity as mice performed the task. The prevalence and strength of alpha phase modulation differed significantly across regions and between cell types. Phase-modulated neurons exhibited greater changes in spiking activity during task execution than their unmodulated counterparts. Furthermore, alpha modulation of neuronal spiking during baseline activity correlated with task performance. In particular, many neurons selectively exhibited strong alpha modulation of spiking activity prior to correct trials, but not prior to incorrect trials. These data suggest that dysregulation of spiking activity with respect to the ongoing alpha oscillation may characterize lapses in task engagement or attention.

Introduction

Neural oscillations play a critical role in regulating various perceptual and cognitive functions, including sensory processing, memory, attention, and decision-making. They serve as a mechanism for coordinating communication between different neural circuits (Gray et al., 1989; Buzsáki and Draguhn, 2004; Weiss et al., 2023). Since the advent of electroencephalography (EEG), alpha oscillations (8-12 Hz, ranges vary depending on the study) have been the object of close study (Berger, 1929; Ojha, 2024). Alpha oscillations have been observed in diverse cortical regions, including visual, somatosensory, motor, premotor, auditory, and entorhinal cortices (da Silva et al., 1973; Steriade et al., 1990; Lehtelä et al., 1997; Lukatch and MacIver, 1997; Castro-Alamancos and Tawara-Hirata, 2007; Haegens et al., 2011). Because alpha oscillations are most prominent in visual cortex with eyes closed, they were previously hypothesized to represent an idling state and were therefore inessential for understanding cognition (Adrian and Matthews, 1934; Steriade et al., 1990; Worden et al., 2000). However, there is strong evidence that alpha oscillations play a functional role in cognitive processing with rhythmic inhibition suppressing the representation and processing of task-irrelevant stimuli (Cooper et al., 2003; Klimesch et al., 2007; Palva and Palva, 2007). Lateralization of alpha oscillations in spatial attention tasks, with high alpha power in task-relevant regions ipsilateral to attended stimuli and low alpha power in task-relevant regions contralateral to attended stimuli, provide further support for the role of alpha in suppressing irrelevant representations (Jensen and Mazaheri, 2010; Händel et al., 2011; Wildegger et al., 2017; Dahl et al., 2019; Schneider et al., 2019; Bagherzadeh et al., 2020). The rhythmic inhibition associated with alpha oscillations may also provide a mechanism by which sensory processing is discretized (VanRullen and Koch, 2003; Mazaheri and Jensen, 2010).

Much of the work on alpha oscillations' role in human cognition has focused on changes in power or synchronization in the EEG over long timescales (on the order of seconds), without regard for the relationship between neuronal firing and the alpha rhythm on the timescale of an alpha cycle (~80 - 125 ms). However, several studies have demonstrated phase locking of neuronal firing to cortical alpha oscillations in monkeys, demonstrating coupling of cortical spiking activity to the phase of the alpha cycle in local field potentials (LFP) (Bollimunta et al., 2008; Bollimunta et al., 2011; Buffalo et al., 2011; Haegens et al., 2011; van Kerkoerle et al., 2014; Dougherty et al., 2017). Cortical firing activity was shown to be elevated at the troughs of alpha oscillations and decreased during the peaks, supporting the rhythmic inhibition hypothesis (Haegens et al., 2011). The origins of alpha oscillations, and the identities of the neurons that serve as pacemakers for that rhythm, vary by cortical region (Lukatch and MacIver, 1997; Jones et al., 2000; Bollimunta et al., 2008; Bollimunta et al., 2011). Alpha phase modulation of spiking activity in the primary visual cortex has been shown to regulate visually driven responses (Dougherty et al., 2017). Other studies have investigated the phase locking of cortical spiking activity to alpha, other oscillatory bands in the LFP, or to a "generalized" LFP phase (5 - 50 Hz) and showed differences in the prevalence and strength of phase modulation change with cortical layer (Lakatos et al., 2005; Bollimunta et al., 2008; Davis et al., 2023).

Despite the extensive work on alpha modulation of cortical spiking activity in nonhuman primates, the phenomenon remains largely unexplored in other mammals and brain regions. Additionally,

most studies of alpha phase modulation in nonhuman primates focused on evoked multi-unit activity, without distinguishing which cell types were coupled to the alpha oscillation (Bollimunta et al., 2008; Bollimunta et al., 2011; Buffalo et al., 2011; Haegens et al., 2011; van Kerkoerle et al., 2014; Dougherty et al., 2017). We therefore used Neuropixels probes to record LFPs and single-unit spiking activity in task-relevant brain regions of mice as they performed a whisker-based selective detection task based on Aruljothi et al. (2020) and quantified the modulation of single neurons' baseline spiking activity by the phase of alpha oscillations. We found differences in the prevalence and strength of alpha phase modulation between brain regions (somatosensory cortex, prefrontal cortex, striatum, and amygdala), between cell types within those regions, and along dorsoventral axes within cortical regions. We found that phase-modulated neurons exhibited increased task-related changes in firing rate compared to neurons that were not phase modulated, and we explored how phase modulation of spiking activity mapped onto task performance. Our results suggest that alpha phase modulation of neuronal firing during spontaneous activity promotes representation of, and correct responses to, behaviorally relevant stimuli.

Methods

All experimental procedures were approved by the Columbia University Institutional Animal Care and Use Committee (IACUC) and were conducted in compliance with NIH guidelines. Adult mice of both sexes (3 females, 1 male), aged 3 - 12 months, were used in the experiments. All mice were kept under a 12-hour light-dark cycle. All software used for controlling the behavioral apparatus and data analysis can be found at https://github.com/Neural-Control-Engineering/n-CORTex which contains project-specific code, and https://github.com/Neural-Control-Engineering/AlphaModulation_SelectiveDetection which provides general purpose tools for neurophysiological and behavioral data collection and segmentation.

Surgical procedures

Animals were anesthetized with isoflurane in oxygen (5% induction, 1-2% maintenance) and fixed in a stereotaxic frame (David Kopf Instruments, CA). Body temperature was maintained at 37℃ using a feedback-controlled heating pad (FHC, Bowdoinham, ME). When the animal's condition stabilized, buprenorphine (0.05 mg/kg) was administered subcutaneously before an incision on the scalp was made. Each mouse was implanted with a Neuropixels 1.0 multielectrode encased in a custom built headstage housing designed for chronic head-fixed recordings (Liu et al., 2024) (**Fig. 2A**). Probe trajectories were planned and monitored in real-time during implantation using Neuropixels Trajectory Explorer (https://github.com/petersaj/neuropixels_trajectory_explorer, by Andy Peters). Two mice were implanted with probes spanning primary somatosensory cortex, striatum (dorsal striatum / caudoputamen and small portions of ventral striatum), and basolateral amygdala contralateral to the side where go stimuli were presented (see Behavioral task below) (**Fig. 2A, B**). Two other mice were implanted with a probe in medial prefrontal cortex (primarily infragranular layers of anterior cingulate, pre- and infralimbic, orbitomedial, and dorsal peduncular cortices) (**Fig. 2B**) contralateral to the go stimulus. Baytril (5 mg/kg) and Carprofen (5 mg/kg) were administered at the end of the surgery and every 24 hours after the surgery for four days. Animals' weight was measured once a day during this post-operative period.

Behavioral task

Head-fixed mice (n=4) were trained to perform a whisker-based go/no-go selective detection task based on Aruljothi et al. (2020). During behavioral training mice were water restricted to maintain ≥ 85% of their post-surgery body weight. Mice had ad libitum access to food. The behavioral apparatus was controlled by custom code written in MATLAB and Simulink (MathWorks, Natick, MA) via a Speedgoat real-time system (Speedgoat Inc., Natick, MA). Trials began with a unilateral whisker deflection lasting 200 ms delivered via a piezoelectric actuator connected to a flat paddle which made contact with multiple whiskers. The tactile stimulus was a triangle wave with 1 mm amplitude, 100 ms of rise time, and 100 ms of fall time (**Fig. 1**). Mice were required to selectively respond to left-sided whisker deflections (go stimuli) by licking a water spout within a 1 s window of opportunity in order to receive a water reward, and they were required to ignore right-sided whisker deflections (no-go stimuli). Failure to withhold licks during the window of opportunity following a no-go stimulus resulted in an increased inter-trial interval (8-12 s with a negative exponential distribution, as opposed to 4-8 s otherwise). On any given trial, the probability of a go stimulus presentation was 30%; the probability of a no-go stimulus was 70%. Mice had to withhold licks during the 200 ms of stimulus delivery. Licking during this period voided the trial (it was not included in further analyses), and mice did not receive water reward regardless of the side on which the stimulus was delivered. Sessions lasted one hour. All mice achieved expert performance on the task, defined as 3 consecutive sessions with perceptual sensitivity (d') greater than 1, and we included sessions after and including the first session in that 3-session streak (**Fig 1D**).

Neural recordings

Neural signals across 384 electrodes of the Neuropixels 1.0 probe were recorded while the mice performed the selective detection task using a National Instruments PXI system controlled by SpikeGLX (Release v20230905-phase30). The recording system was synchronized with the behavioral apparatus via TTL pulses generated by the Speedgoat real-time system. The behavioral task and neural recordings were performed in a box lined with copper mesh to reduce electromagnetic noise. Software wrote data to disk in two separate binary files: one containing a wide-band signal (0.3-10 kHz bandwidth, 30 kHz sampling rate, 250x gain) and the other a lower band signal (0.5-500 Hz bandwidth, 2.5 kHz sampling rate, 125x gain) for analysis of the local field potential (LFP). Single-unit spiking activity was extracted offline using Kilosort 4.0 (Pachitariu et al., 2024). Only single-units labelled 'good' by Kilosort 4.0 with physiologically realistic inter-spike intervals were used in further analysis. Local field potentials (LFPs) were downsampled to 500 Hz after applying a fourth order Butterworth bandpass anti-aliasing filter with cutoff frequencies at 0.1 Hz and 100 Hz using forward and backward passes (MATLAB's *filtfilt)*.

Analysis

Individual neurons were classified by their waveform templates identified by Kilosort 4.0. Positive spiking units, characterized by positive deflections in the extracellular waveform and likely representing axonal spikes, and triphasic spiking units, characterized by small positive deflections preceding larger negative deflections and likely representing dendritic spikes, were not included in further analyses (Jung et al., 2023; Someck et al., 2023). The remaining units were classified as regular spiking (RS) and fast spiking (FS) units based on the action potential width and the

time between the trough and subsequent peak of the waveform template using k-means clustering (**Fig. 2C**) (Hocker et al., 2021; Liu et al., 2024). Peristimulus time histograms and firing rates were computed using 50 ms non-overlapping bins. Baseline multitaper LFP spectra (time-bandwidth product 5, 9 tapers) were computed using the Chronux toolbox (http://chronux.org/) (Mitra and Bokil, 2007). We also analyzed the aperiodic (1/f-like dynamics) and periodic (local peaks in the spectrum) components of averaged spectrograms using an algorithm developed by Donoghue et al. (2020) (https://github.com/fooof-tools/fooof). For each session, we averaged baseline LFP spectra across trials of each outcome, identified local peaks in the averaged spectra, and computed the relative power (to the rest of the spectrum) and bandwidth of those peaks.

Alpha band activity in the LFP was isolated by bandpass filtering the raw LFP signal from 8 to 12 Hz with a fourth order non-causal Butterworth filter (MATLAB's *filtfilt)* to avoid imposing spurious phase shifts. The instantaneous phase of the alpha band was computed using the Hilbert transform. Spikes were then registered to the instantaneous phase of alpha on the electrode where the spike waveform produced the greatest deflection. To identify neurons whose baseline activity was significantly modulated by alpha phase, we pooled the instantaneous phases of all baseline (3 s before stimulus) spikes across the session and used Rayleigh's test for non-uniformity (Fisher, 1993). Units were considered significantly phase modulated if the p-value from Rayleigh's test was less than 0.05 divided by the number of units recorded on a given session (Bonferroni correction for multiple comparisons). To quantify alpha modulation of spiking activity, we fit von Mises distributions (circular analog of normal distribution) to the probability density function of spikes in 20 18° bins of alpha phase (Eschenko et al., 2012). A similar procedure was used to identify whether units were phase modulated prior to trials of various outcomes, only including instantaneous phases of baseline spikes on trials of a given outcome. The same corrected p-value threshold was used to identify significant phase modulation prior to trials with different outcomes. Comparisons of preferred phase between cell types and regions were performed using Kuiper's test (Fisher, 1993). We computed the mean squared error (MSE) between the best fit von Mises distribution and the observed distribution to quantify how much alpha modulation of spiking activity deviated from a "normal" distribution. We also computed the modulation index (MI) to quantify how the observed distributions of spikes relative to alpha phase deviated from a uniform distribution (Tort et al., 2010; Dougherty et al., 2017):

$$MI = \frac{\log(N) - \left(-\sum_{j=1}^{N} P(j)\log|P(j)|\right)}{\log(N)}$$

Here, *j* is a single phase bin and *P(j)* is the normalized spike count in that bin. For the handful of neurons that exhibited bimodal distributions of spiking probability relative to alpha phase, we fit a mixture of two Gaussian distributions.

We also compared alpha phase modulation during oscillatory events with high and low alpha power during spontaneous activity (3 s). For each phase modulated neuron, we computed instantaneous alpha power on the electrode where that neuron was recorded using bandpass filtering and the Hilbert transform as above. We identified epochs 0.3 s or longer where alpha power was greater than or equal to the 75th percentile of alpha power across the session on that electrode as high alpha events and epochs 0.3 s or longer where alpha power was less than the 50th percentile of alpha power across the session as a low alpha event. When there was an

interval between events of the same kind 0.2 s or shorter, those events were combined. We then analyzed phase modulation of spiking activity across high alpha power events and low alpha power events separately.

Statistics

All circular statistics were performed using the CircStat toolbox for MATLAB (Berens 2009). We used Rayleigh's test for non-uniformity to determine which neurons were significantly modulated by alpha phase. We used Kuiper's test to compare distributions of preferred phase angles of spiking activity (Fisher, 1993). Watson-Williams test was used as a circular analog of ANOVA (Berens 2009). For non-circular data, we tested for homoscedasticity using the Kolmogorov-Smirnov test. If data were not normally distributed, we used nonparametric tests (Wilcoxon signed-rank test and Mann-Whitney U-test) where applicable.

Results

We trained head-fixed mice (n=4) to perform a whisker-based selective detection task, requiring mice lick in response to left-sided whisker deflections (go stimuli) to receive a water reward and withhold licks in response to right-sided whisker deflection (no-go stimuli) to avoid a longer inter-trial interval (**Fig. 1A**). Performance was evaluated using discriminability (d') from signal detection theory (Stanislaw and Todorov, 1999). The average d' across all sessions was 2.32 ± 0.16 (SEM unless otherwise noted), with hit rates (86.0 ± 3.3%) significantly higher than false alarm rates (16.3 ± 2.2%) (**Fig. 1B**; $p = 2.6 \times 10^{-18}$, paired t-test). Reaction times did not differ significantly between false alarm trials (0.50 ± 0.05 s) and hit trials (0.64 ± 0.05 s; p = 0.60, paired t-test; **Fig. 1C**).

We recorded neural activity during expert task performance across 28 sessions with chronically implanted Neuropixels 1.0 probes (**Fig. 2A**). Probe trajectories spanned primary somatosensory/barrel cortex (S1), striatum (mostly dorsal striatum / caudoputamen), and amygdala (lateral and basolateral amygdala) in 2 mice and prefrontal cortex (PFC) in 2 other mice (**Fig. 2B**). All probes were implanted contralateral to the go stimulus. We identified single-units in each recording using Kilosort 4.0 and classified them based on their waveform templates (Pachitariu et al., 2024). We used k-means to classify single-units as fast spiking (FS) and regular spiking (RS) based on their action potential half widths and the time from the trough to the subsequent peak of the waveform (**Fig. 2B**). 73.2% of units in S1 were classified as RS units while 26.8% of units were classified as FS units. 92.5% of units in PFC were classified as RS units while 7.5% of units were classified as FS units. Proportions of FS and RS units recorded were in line with previous observations in S1 and PFC (Agmon and Connors, 1992; Liu et al., 2024). In the striatum, 55.2% of units were classified as RSUs, while 44.8% were classified as FSUs. This was a more equal distribution than previous observations from striatum in rats and monkeys (Gage et al., 2010; Yamada et al., 2016). 20.2% of units in amygdala were classified as RS units and 79.8% were classified as FS units. Previous work found a higher percentage of FS units in amygdala in rats but used firing rate rather than waveform shape to classify units (Rosenkranz and Grace, 1999).

Subpopulations in each recorded region exhibited task-related spiking dynamics during task execution and differences in stimulus-evoked changes in spiking activity during the 200 ms decision period between stimulus presentation and acceptable motor response (**Fig. 2D,E**). We focused on comparisons between hit and miss trials because neural recordings were aligned (contralateral) to the go-stimulus. FS units in S1 showed significantly greater stimulus-evoked increases in firing rate from baseline during hit trials (10.6 ± 1.1 Hz) than on miss trials (7.1 ± 1.1 Hz; $p = 2.46 \times 10^{-6}$, Wilcoxon signed-rank test), while there was no significant difference in stimulus-evoked activity in S1 RS units (2.7 ± 0.3 Hz on hit trials, 2.5 ± 0.3 Hz on miss trials, p = 0.10, Wilcoxon signed-rank test). In PFC, neither RS or FS units exhibited significantly different changes in stimulus-evoked firing on hit versus miss trials (p = 0.40, p = 0.52, Wilcoxon signed-rank test, respectively). In striatum, RS units exhibited significantly greater stimulus-evoked increases in firing rate on hit trials (5.3 ± 1.0 Hz) than on miss trials (4.5 ± 0.8 Hz; p = 0.001, Wilcoxon signed-rank test), while there was no significant difference for FS units (5.8 ± 0.6 Hz on hit trials, 5.8 ± 0.6 Hz on miss trials; p = 0.71, Wilcoxon signed-rank test). Finally, in amygdala, FS units showed significantly greater stimulus-evoked increases in firing rate on hit trials (6.5 ± 1.2 Hz) than on miss trials (4.0 ± 0.9 Hz; p = 0.002, Wilcoxon signed-rank test), while there was no significant difference for RS units (12.7 ± 4.8 Hz for hit, 8.2 ± 2.8 Hz for miss; p = 0.31, Wilcoxon signed-rank test). FS and RS units in all regions also exhibited reward-related changes in firing rate. On hit trials, firing rates exhibit local maxima immediately following reward, with the most prominent increases in firing rate occurring in FS units in striatum, amygdala, and PFC. These differences in firing rates among regions, trial outcomes, and cell types were observed following stimulus presentation, but firing rates during baseline activity alone in any given cell population were not predictive of trial outcome.

In addition to single-unit activity, we recorded LFPs from all channels across the probes (**Fig. 2F-H**). In S1, striatum, and amygdala, there was little difference in the spectra of baseline LFPs (1 s prior to stimulus) between the different trial outcomes. We did, however, observe a significant overall reduction in spectral power ($p = 5.90 \times 10^{-16}$, 2-way ANOVA) and an increase in the slope of the spectrum in PFC prior to miss trials compared to hit trials (**Fig. 2F**). Averaging spectra like this can mask features like local peaks, so we employed a method which separately parameterized the aperiodic components (1/f-like dynamics) and periodic components (local peaks) of LFP spectra (Donoghue et al., 2020). We identified periodic components in baseline LFP spectra averaged across trials of each outcome in each session. Periodic components in the alpha range (~8 Hz in S1, ~10 Hz elsewhere) were common; however, on average the center-frequency of local peaks in the spectra tended to be higher (high alpha or beta frequencies), while their relative power tended to be lower, prior to miss trials compared to other outcomes (11.0 ± 1.4 Hz in S1, 16 ± 2.4 Hz in PFC, 14.3 ± 2.1 Hz in striatum, and 14.4 ± 2.2 Hz in amygdala (**Fig. 2G**). Since we were particularly interested in the relationship between spiking activity and the phase of alpha oscillations, we measured the average phase shift in the alpha band between a reference electrode (in layer 5 for the S1-striatum-amygdala implants and in prelimbic cortex (PL) for the PFC implants) and all other electrodes along the probe during baseline activity (3 s prior to stimulus) across all trials (**Fig. 2H**). There was little phase shift in the alpha band within S1 (except on the most superficial electrodes) and PFC relative to the reference electrodes, but there

was a fairly uniform phase shift of ~ 1 radian in striatum and amygdala relative to their reference electrode in layer 5 of S1.

Alpha phase modulation of single-unit spiking across brain regions

Even during brief time windows, the timing of spiking activity in some neurons exhibited a clear relationship with the phase of the alpha oscillation. **Figure 3A** shows a single example neuron, specifically an FS unit from S1, whose spiking activity was significantly modulated by the phase of an ongoing alpha oscillation (8 - 12 Hz) during 3s of baseline activity prior to a hit trial ($p = 0.002$, Rayleigh's test). The LFP recorded on the same channel as the neuron was bandpass filtered from 8 - 12 Hz (**Fig. 3A top**), and the instantaneous phase of the alpha band was computed using the Hilbert transform (**Fig. 3A center**). Spikes were then registered to the instantaneous phase of the alpha oscillation. To visualize the distribution of spikes, we computed the probability density of spiking at binned phases of alpha and fit a von Mises distribution (circular analog of normal distribution) (**Fig. 3A bottom**). To identify neurons whose baseline activity was significantly alpha phase modulated over the course of the whole session, we pooled the instantaneous alpha phases of all spikes during 3 seconds of baseline activity across all trials, regardless of outcome (360 trials or 18 minutes of baseline activity, on average) and performed Rayleigh's test for nonuniformity for all single-units recorded. If the p-value from Rayleigh's test was less than 0.05 divided by the number of single-units recorded on a given session, that neuron was considered significantly phase modulated.

Phase modulation of single neuron spiking activity was commonplace in neocortex and comparatively rare in subcortical regions (**Fig. 3B**). Phase-modulated RS units were significantly more common in S1 than in PFC, striatum, and amygdala ($p = 1.09 \times 10^{-4}$, Mann Whitney U-test; $p = 6.10 \times 10^{-5}$, $p = 0.039$, Wilcoxon signed rank; respectively). Phase-modulated FS units were significantly more common in S1 than in striatum and amygdala but not PFC ($p = 1.22 \times 10^{-4}$, $p = 0.025$, Wilcoxon signed-rank test; 0.363 Mann Whitney U-test; respectively). Both RS and FS units were significantly more common in PFC than in striatum ($p = 1.44 \times 10^{-5}$, $p = 6.39 \times 10^{-6}$, Mann Whitney U-test, respectively). FS units, but not RS units, were significantly more common in PFC than in amygdala ($p = 0.002$, $p = 0.199$, Mann Whitney U-test, respectively). There were no significant differences in the prevalence of phase modulation in striatum compared to amygdala for RS or FS units ($p = 0.742$, $p = 0.457$, Wilcoxon signed-rank test, respectively). For most significantly phase-modulated neurons, the distribution of spikes across alpha phase was well characterized by a von Mises distribution (e.g., **Fig. 3C**, left and center); however, a small number of neurons in PFC (2.5% of RS units and 4.0% of FS units) were better characterized by a bimodal distribution (e.g., **Fig. 3C**, right).

In S1, 62.1 ± 5.8% of RS units per session and 63.2 ± 6.0% of FS units per session were significantly phase modulated. We computed the preferred phase of spiking for each alpha modulated neuron by computing the circular mean across the instantaneous alpha phases at each spike time. The distribution of preferred phases for phase-modulated RS units (mean of 2.7 ± 0.05 radians) differed significantly from the distribution of preferred phases of phase-modulated FS units (mean of 3.0 ± 0.09 radians; $p = 0.01$, Kuiper's test). We compared task-related changes in firing rates during task execution (1.2 s following stimulus onset) between alpha phase-

modulated neurons and unmodulated neurons. There was no difference in task-related changes in spiking dynamics between modulated and unmodulated S1 RS cells on hit trials ($p = 0.38$, 2-way ANOVA). There was, however, a significant difference in task-related changes in firing rate between modulated and unmodulated S1 FS units on hit trials ($p = 3.50 \times 10^{-9}$, 2-way ANOVA), with greater stimulus-evoked firing rate increases and elevated firing rates following reward in phase-modulated units compared to unmodulated units on hit trials. There was no difference in modulation index (MI, deviation from uniform distribution) between phase-modulated FS and RS units ($p = 0.11$, Mann-Whitney U-test), but there was significantly higher mean squared error (MSE) of the best fit von Mises distribution (deviation from the circular analog of a normal distribution) for phase-modulated RS units ($2.6 \times 10^{-4} \pm 4.4 \times 10^{-5}$) than FS units ($8.0 \times 10^{-5} \pm 2.6 \times 10^{-5}$; $p = 3.0 \times 10^{-10}$, Mann-Whitney U-test) (**Fig. 3C**).

In PFC, we recorded a significantly higher fraction of alpha modulated FS units (75.3 ± 7.0% per session) than RS units (25.2 ± 2.1% per session; $p = 2.44 \times 10^{-4}$, Wilcoxon signed rank test). The distribution of preferred phases for phase-modulated RS units (mean of 2.8 ± 0.06 radians) differed significantly from that of phase-modulated FS units (mean of -1.3 ± 0.23 radians; $p = 0.001$, Kuiper's test). Phase-modulated FS units were more evenly split between those who spiked most often at the peak of the alpha wave and those that spiked most often at the trough, while by far most RS units spiked most often at the trough of the alpha wave. For both RS and FS units, phase-modulated neurons exhibited significantly greater task-related changes in firing rate dynamics on hit trials than unmodulated units ($p = 4.3 \times 10^{-30}$, $p = 3.8 \times 10^{-17}$, respectively, 2-way ANOVA). Alpha phase-modulated units of both classes exhibited strong local peaks in firing rate following stimulus and reward on hit trials compared to their unmodulated counterparts. Phase-modulated RS units exhibited significantly higher MI ($0.012 \pm 9.1 \times 10^{-4}$) and MSE ($5.5 \times 10^{-4} \pm 7.2 \times 10^{-5}$) than phase-modulated FS units (MI: $6.4 \times 10^{-3} \pm 6.3 \times 10^{-4}$; $p = 1.3 \times 10^{-4}$, Mann-Whitney U-test; MSE: $1.3 \times 10^{-4} \pm 6.4 \times 10^{-5}$; $p = 2.1 \times 10^{-9}$, Mann-Whitney U-test). Considering that the MSEs of the best fit von Mises distributions for both FS and RS units were fairly small, the higher MI for RS units suggests they are more strongly modulated by alpha phase than FS units (**Fig. 3D**).

Phase-modulated units were rare in striatum compared to neocortex, with 4.1 ± 1.7% RS units per session exhibiting significant phase modulation and 9.2 ± 2.6% FS units per session exhibiting significant phase modulation. The fraction of alpha modulated FS units was significantly higher than the fraction of alpha modulated RS units ($p = 0.004$, Wilcoxon signed rank test). There was no significant difference in the preferred phase distributions between RS units (mean of -2.8 ± 0.15 radians) and FS units (mean of -2.7 ± 0.20 radians) in striatum. There were significant differences in task-related changes in firing rate between phase-modulated and unmodulated FS units ($p = 7.9 \times 10^{-28}$, 2-way ANOVA) and RS units ($p = 2.8 \times 10^{-78}$, 2-way ANOVA). Interestingly, unmodulated FS units exhibited a more prominent local peak in firing rate following reward compared to phase-modulated FS units, suggesting that in striatum phase-modulated FS units play a greater role in stimulus representation while unmodulated FS units play a greater role in reward processing. Similar to PFC, phase-modulated RS units exhibited significantly higher MI ($0.015 \pm 4.6 \times 10^{-4}$) and MSE ($6.2 \times 10^{-4} \pm 2.9 \times 10^{-5}$) than phase-modulated FS units (MI: $6.0 \times 10^{-3} \pm 7.3 \times 10^{-4}$; $p = 0.004$, Mann-Whitney U-test; MSE: $7.1 \times 10^{-5} \pm 2.2 \times 10^{-5}$; $p = 2.4 \times 10^{-4}$,

Mann-Whitney U-test). However, MSEs of the best fit von Mises distributions were fairly high for RS units, suggesting that phase-modulated FS unit activity was more tightly coupled to the phase of alpha oscillations than RS unit activity (**Fig. 3E**).

Compared to other regions, we recorded very few significantly phase-modulated RS or FS units in amygdala (3 and 9 in total across all sessions, respectively). 33.3 ± 16.7% of recorded RS units per session were phase modulated, and 25 ± 9.9% of FS units per session were phase modulated. There was no significant difference in the preferred phase distributions between RS units (mean of -0.66 ± 0.39 radians) and FS units (mean of -0.82 ± 0.28 radians) in amygdala. There were significant differences in task-related changes in spiking dynamics between phase-modulated and unmodulated FS units ($p = 1.0 \times 10^{-6}$, 2-way ANOVA) and RS units ($p = 1.2 \times 10^{-52}$, 2-way ANOVA with repeated measures). RS and FS units in amygdala did not show significant differences in either MI or MSE ($p = 1.00$, $p = 0.483$, Mann Whitney U-test, respectively) (**Fig. 3E**).

Dorsoventral distributions of phase modulation in S1 and PFC

The prevalence and strength of phase modulation varied along the dorsoventral axis in S1 and PFC (**Fig. 4**). Approximate layers in S1 and subregions of PFC were assigned by monitoring electrode position in real-time using Neuropixels Trajectory Explorer during implantation (see Methods). In S1, the fraction of both RS and FS units which were modulated by alpha phase differed significantly across cortical layers ($p = 8.66 \times 10^{-9}$, $p = 2.77 \times 10^{-4}$, one-way ANOVA, respectively) (**Fig. 4A)**. For both FS and RS units, alpha modulation was rare in layer 1 but widespread in layers 2 through 4. Phase-modulated RS units were common in layer 5 and fell off dramatically in layer 6. Phase-modulated FS units, by contrast, became progressively less common from layer 4 through layer 6. The high incidence of alpha phase modulation in granular cortex compared to infragranular cortex is consistent with previous observations in macaque primary visual cortex (Dougherty et al., 2017). MI varied significantly across cortical layers for both RS ($p = 7.8 \times 10^{-10}$, one-way ANOVA) and FS units ($p = 3.4 \times 10^{-4}$, one-way ANOVA), with the highest MIs observed in layer 2/3 RS units (0.23 ± 0.003). Similarly, MSE varied significantly across cortical layers for both RS ($p = 1.1 \times 10^{-5}$, one-way ANOVA) and FS units ($p = 6.6 \times 10^{-4}$, one-way ANOVA), with the highest MSEs observed in layer 2/3 RS units ($8.4 \times 10^{-4} \pm 2.7 \times 10^{-4}$). Even though layer 2/3 units exhibited the highest MSEs, they were still very well characterized by von Mises distributions, so based on those neurons having the highest MI, we can surmise that layer 2/3 RS unit activity was more strongly modulated by the phase of alpha oscillations than any other population in S1. Finally, the preferred alpha phase of spiking changed significantly with cortical depth (RS: $p = 6.01 \times 10^{-12}$, FS: $p = 2.03 \times 10^{-6}$, Watson-Williams test). Phase-modulated RS in deeper layers of cortex (layers 4-6) tended to spike most often before the minimum of the trough in the alpha wave, and those in superficial layers tended to spike after the minimum of the trough. FS units did not exhibit the same trend, but alpha modulated FS units in layers 5 and 6 also tended to spike most often following the trough of the alpha wave. Correlations between phase modulation and task-related spiking dynamics also varied across cortical layers (**Fig. 4B**). Generally, FS units across cortical layers exhibited greater differences in task-related spiking activity between modulated and unmodulated units than observed in RS units.

Probes implanted in PFC spanned a number of subregions in PFC but were located entirely in infragranular layers. The prevalence of phase modulation also varied significantly between subregions of PFC among RS ($p = 1.77 \times 10^{-4}$, one-way ANOVA) and FS units ($p = 0.007$, one-way ANOVA) (**Fig. 4C**). Phase-modulated RS units were rare in anterior cingulate cortex (ACC; 5.3 ± 1.7%) and orbitomedial cortex (ORB; 1.5 ± 0.9%) and most common in infralimbic cortex (IL; 54.0 ± 9.9%). Phase-modulated FS units followed their own distribution, with high prevalence in ACC (85.7 ± 0.09%) and IL (100% across all sessions). MI varied significantly across subregions of PFC for RS and FS units ($p = 3.07 \times 10^{-6}$, $p = 0.014$, one-way ANOVA, respectively). MSE, however, only varied significantly across subregions in phase-modulated RS units ($p = 0.025$, one-way ANOVA). Phase-modulated FS units, by contrast, exhibited fairly uniform MSE across subregions ($p = 0.46$, one-way ANOVA). Compared to S1, the phase of alpha at which neurons fired most often varied considerably across subregions (RS: $p = 4.77 \times 10^{-4}$, FS: $p = 0.160$, Watson-Williams test). For RS units in ORB, FS units in DP, and units of both classes in ACC, the average phase at which those neurons fired was close to 0 radians (spikes occurred most frequently around the peak of the alpha oscillation). Phase-modulated neurons like this are not completely absent from S1 or other subregions of PFC, but they are far less prevalent and only found in infragranular layers (**Fig. 3C, D**).

Dynamic changes in alpha power and phase modulation

Since alpha power changes dynamically, even over the course of the 3 s baseline periods of activity on which our analyses have focused, we naturally wondered whether phase modulation of single-unit activity varied with alpha power (**Fig. 5**). To this end, we identified low and high alpha power events during baseline activity on each electrode where we recorded a phase-modulated neuron. Low alpha power events were defined as epochs ≥ 0.3 s where alpha power remained below its 50th percentile (on that electrode across the recording session). Similarly, high alpha power events were defined as epochs ≥ 0.3 s where alpha power remained above its 75th percentile. In an example neuron (**Fig. 5A**), we observed different spike distributions across alpha phase during low- and high-power events. Both were well characterized by a von Mises distribution, but the distribution during high alpha power events deviated much more strongly from a uniform distribution. We compared MI, MSE of the best fit von Mises distribution, average firing rate, and preferred firing phase of alpha across spikes for all phase-modulated RS and FS units during low and high alpha power events (**Fig. 5B**). For RS and FS units across S1, PFC, and striatum, MI increased significantly between low and high alpha power events ($p < 4.3 \times 10^{-6}$, Wilcoxon signed-rank test). Similarly, all units in all regions except RS units in amygdala exhibited significantly higher MSE of the best fit von Mises distributions during high alpha power events than during low alpha power events ($p < 3.9 \times 10^{-3}$, Wilcoxon signed-rank test). Interestingly, there was little difference in firing rates between low and high alpha events. Only striatum FS unit firing rates were significantly higher (0.76 Hz on average) during high alpha events than during low alpha events ($p = 2.4 \times 10^{-3}$, Wilcoxon signed-rank test); otherwise, there were no significant differences in firing rate between high and low alpha power events. This implies that increased alpha power does not simply reflect an increase in rhythmic inhibitory tone, which one might expect to reduce overall firing rate. Instead, the higher MI during high alpha power events, in conjunction with the lack of change in firing rates, suggests that increased alpha power reflects balanced increases in rhythmic excitation and inhibition. Finally, there was little difference in the

average alpha phase across spikes between low and high alpha power events. Only RS units in S1 exhibited significantly different average firing phases during low and high alpha events (0.11 radians higher on average during low events, p = 0.002, Kuiper's test).

Single neuron phase modulation and its relation to behavior

We next investigated how spontaneous (pre-stimulus) alpha modulation of single neuron spiking activity related to cognitive performance (correct vs. incorrect) and motor activity (action vs. inaction) during the selective detection task. To quantify these relationships, for each neuron previously identified as alpha modulated, we pooled the instantaneous alpha phase of each spike across trials of a given outcome: hit, miss, correct rejection, false alarm, correct (hit and correct rejection), incorrect (miss and false alarm), action (hit and false alarm), and inaction (miss and correct rejection). We then computed p-values from the distributions of baseline spike phases of each trial outcome using Rayleigh's test and used the same corrected p-value threshold as above to determine if the neuron's spiking activity was significantly modulated by alpha phase prior to trials of a given outcome. **Figure 6** shows examples of alpha modulated neurons from each region and their relationships between alpha modulation and trial outcome. An example FS unit from S1 exhibited significant alpha phase modulation of spiking activity prior to hit trials and correct rejection trials but not prior to miss trials or false alarm trials. When pooling across correct and incorrect trials, this neuron exhibited significant alpha phase modulation prior to correct trials, but not prior to incorrect trials. When pooling across action trials and inaction trials, this neuron exhibited significant alpha phase modulation regardless of whether the mouse licked or did not lick during the window of opportunity (**Fig. 6A**). Similar patterns of phase modulation, with significant phase modulation prior to correct trials but not incorrect trials, were observed in a number of neurons across recorded regions (**Fig. 6C-D)**.

To systematically investigate the relationship between alpha phase modulation and cognitive performance, we computed the proportion of phase-modulated units of each waveform class (RS or FS) which were selectively phase modulated on correct trials, selectively phase modulated on incorrect trials, or phase modulated regardless of the cognitive outcome of the trials (i.e., phase modulated prior to both correct and incorrect trials). Similarly, to investigate the relationship between alpha phase modulation and motor output, we computed the proportion of phase-modulated units of each waveform class that were selectively phase modulated on action trials, selectively phase modulated on inaction trials, or phase modulated regardless of motor outcome (i.e., phase modulated prior to both action and inaction trials) (**Fig. 7A)**. Neurons which were selectively phase modulated prior to correct trials were the most common across brain regions, while neurons which were phase modulated regardless of trial outcome were less common, and neurons which were selectively phase modulated prior to incorrect trials were extremely rare. By comparison, the differences in proportions of neurons selectively phase modulated prior to action or inaction trials, or those phase modulated prior to both, were less pronounced than when focusing on cognitive outcome.

MI varied significantly across trial outcomes (hit, miss, correct rejection, and false alarm) for both RS and FS units in S1, PFC, and striatum (RS: $p = 2.03 \times 10^{-17}$, $p = 3.07 \times 10^{-6}$, $p = 0.002$; FS: 1.16×10^{-4}, $p = 1.95 \times 10^{-10}$, $p = 0.039$; one-way ANOVA; respectively) (**Fig. 7B**). MI was

significantly higher in both RS and FS units in S1, PFC, and striatum prior to incorrect trials compared to correct trials (RS: $p = 4.64 \times 10^{-25}$, $p = 1.35 \times 10^{-15}$, $p = 1.87 \times 10^{-5}$; FS: $p = 2.70 \times 10^{-6}$, $p = 7.86 \times 10^{-4}$, 2.52×10^{-5}; Wilcoxon signed rank test; respectively). MI was significantly higher prior to action trials compared to inaction trials for RS and FS units in S1 ($p = 6.10 \times 10^{-8}$, $p = 1.73 \times 10^{-3}$, Wilcoxon signed rank test, respectively), RS units in PFC ($p = 6.65 \times 10^{-3}$, Wilcoxon signed rank test), and FS units in striatum ($p = 2.85 \times 10^{-3}$, Wilcoxon signed rank test). In S1, PFC, and striatum, MI varied more strongly between correct and incorrect trials than between action and inaction trials. Similarly, MSE of the best fit von Mises distributions varied significantly by trial outcome (hit, miss, correct rejection, and false alarm) in both RS and FS units in S1, PFC, and striatum (RS: $p = 3.36 \times 10^{-19}$, $p = 6.03 \times 10^{-29}$, $p = 4.72 \times 10^{-4}$; FS: $p = 5.56 \times 10^{-5}$, $p = 3.17 \times 10^{-12}$, $p = 0.028$; one-way ANOVA; respectively) (**Fig. 7C**). MSE of the best fit von Mises distributions were significantly higher prior to incorrect trials than correct trials (RS: $p = 6.90 \times 10^{-31}$, $p = 1.03 \times 10^{-16}$, $p = 8.30 \times 10^{-6}$; FS: $p = 2.83 \times 10^{-6}$, $p = 5.60 \times 10^{-5}$, $p = 3.79 \times 10^{-6}$; Wilcoxon signed rank test; respectively). MSE of the best fit von Mises distributions was significantly higher prior to action trials compared to inaction trials in RS and FS units in S1 ($p = 2.97 \times 10^{-20}$, $p = 8.76 \times 10^{-11}$, Wilcoxon signed rank test, respectively), RS units in PFC ($p = 6.55 \times 10^{-4}$, Wilcoxon signed rank test), and RS and FS units in striatum ($p = 7.65 \times 10^{-4}$, $p = 7.26 \times 10^{-6}$, Wilcoxon signed rank test, respectively). Like MI, MSE of the best fit von Mises distributions varied more strongly between correct and incorrect trials than between action and inaction trials.in S1, PFC, and striatum. While higher MI may be mistaken for stronger coupling, higher MI combined with the magnitude of MSE observed on incorrect trials (compare to MSE in **Figs. 3-5**) is better explained by an increased randomness in the relationship between spiking activity and alpha phase as seen in the examples from **Figure 6** - strong deviation from both uniform and normal distributions. Taken together, these data suggest that poor cognitive performance on the task was preceded by disruptions in the modulation of single-unit spiking activity by the phase of alpha oscillations. There were, however, no significant differences in average preferred spiking phases between cognitive or motor outcomes (**Fig. 7D**).

Discussion

The physiology of spontaneous alpha modulation

In this study, we systematically characterized alpha modulation of single-unit spiking activity in two cortical (S1 and PFC) and two subcortical (striatum and amygdala) brain regions during baseline activity associated with different behavioral outcomes. We found phase-modulated neurons in each brain region, but they were far more prevalent in neocortex than in striatum or amygdala (**Fig. 3**). Phase-modulated neurons were also more common in S1 than in PFC; however, all neurons recorded from PFC were located in infragranular layers, whereas neurons recorded from S1 were distributed across all cortical layers. Within PFC, we found significant differences in the prevalence of phase modulation among its subregions (ACC, PL, IL, etc.; **Fig 4C**). Differences in the prevalence of alpha modulation between cortical regions have also been reported in macaques (Bollimunta et al., 2008; Haegens et al., 2011). Within S1, we found the prevalence and strength of alpha modulation differed significantly between cortical layers (**Fig. 4A**). Studies of phase modulation of multi-unit spiking in nonhuman primates also observed laminar differences in the prevalence of phase modulation (Bollimunta et al., 2008; Dougherty et al., 2017; Davis et al., 2023). Bollimunta et al. (2008) observed the weakest coupling between

alpha and multi-unit activity in supragranular layers of higher order visual areas (V2 and V4) in macaques, while Davis et al. (2023) observed the strongest coupling between generalized oscillatory phase (5 - 50 Hz) and multi-unit spiking across PFC and medial temporal lobe in marmosets and V4 of macaques. We observed very sparse alpha modulation in layer 1, but most neurons in layer 2/3 were alpha modulated. It may be that multi-unit activity recordings in supragranular cortex from Bollimunta et al. (2008) were dominated by layer 1 neurons, and recordings from Davis et al. (2023) were dominated by layer 2/3 neurons, if in fact the laminar distributions of phase modulation are comparable between mice and monkeys.

The majority of phase-modulated neurons exhibited distributions of spikes across alpha phase which closely followed a von Mises distribution (a normal distribution in circular space). In other words, these neurons preferentially fired at a particular phase of the alpha cycle (**Fig 3C**). In neocortex, most neurons fired most often at the trough of the alpha cycle (**Fig. 3D, E**) in line with previous findings of alpha modulation of cortical multi-unit spiking in nonhuman primates (Bollimunta et al., 2008; Haegens et al., 2011; van Kerkoerle et al., 2014; Dougherty et al., 2017). This was also true for phase-modulated neurons in striatum (**Fig. 3F**). In S1 and PFC, a small fraction of both RS and FS units preferentially fired near the peak of the alpha cycle, however (**Fig. 3D, E**). All the neurons recorded in PFC were in infragranular layers, but even in S1, where our recordings spanned all cortical layers, all of the neurons that preferentially fired near the peak of the alpha cycle were infragranular. FS neurons that preferentially fired near the peak of the alpha cycle were likely GABAergic interneurons which generated the pulsed inhibition necessary for the more common variety of alpha modulation (Mazaheri and Jensen, 2010). The RS units that preferentially fired at the peak of alpha may have been somatostatin-expressing interneurons, which are commonly found in layer 5 (Xu et al., 2010; Riedemann, 2019), also generating pulsed inhibition. Alternatively, those RS units may have been layer 5 pyramidal neurons expressing h- and T-currents which can both generate and pace the alpha rhythm (Jones et al., 2000). There were a number RS and FS units in striatum that preferentially fired near the peak of the alpha cycle (**Fig. 3F**), but it is unclear whether these neurons generated alpha modulation locally or if their modulated spiking distributions were inherited from elsewhere, particularly neocortex. The small number of phase-modulated neurons in amygdala preferentially fired at neither the peak nor the trough of the alpha oscillation (**Fig. 3G**). Finally, a small number of neurons in PFC exhibited a bimodal distribution with respect to alpha phase (**Fig. 3C**). This variety of phase modulation does not fit neatly into the framework of pulsed inhibition during the peak of the alpha cycle. The mechanism by which this form of coupling arises remains an open question.

Phase-modulated neurons across brain regions exhibited greater task-related changes in firing rate from baseline than their unmodulated counterparts (**Fig. 3D-G**). We hypothesize that the pulsed inhibition responsible for alpha modulation kept neurons' firing rates near the minimum of their dynamic ranges such that tactile stimuli produced greater changes in firing rate. In this sense, the pulsed inhibition associated with alpha oscillations recruits a population of neurons primed to encode sensory stimuli. Interestingly, alpha modulated neurons, particularly in neocortex, also exhibited higher changes in firing rate from baseline after reward delivery compared to their unmodulated counterparts. Whether these signals are related to reward processing or simply the motor activity associated with licking to collect the water reward, this increased activity suggests

that neurons modulated by alpha phase tend to be driven by more diverse sources than sensory stimuli alone.

We observed stronger alpha modulation of spiking activity during events with sustained high alpha power than during events with sustained low alpha power (**Fig. 5**), supporting the pulsed inhibition hypothesis of alpha oscillations (Klimesch et al., 2007; Mazaheri and Jensen, 2010; Mathewson et al., 2011). Even though the MSEs of the best fit von Mises distributions were significantly higher during high alpha events alongside the increased MI (**Fig 5B, C**), it is important to note that the von Mises distribution can take the form of a uniform distribution, as it approached in the example distribution across low alpha events (**Fig. 5A**). In addition, the magnitude of the MSE of the best fit von Mises distributions remained fairly low (compare to the MSE of best fit von Mises distributions for incorrect trials **Fig. 7A, C**). Interestingly, the increased alpha modulation from low to high alpha events was accompanied by negligible changes in firing rate and preferred phase (**Fig 5C**). This suggests that increased pulse inhibition during high alpha events may be accompanied by balanced antiphase pulses of excitation, requiring an amendment to the pulsed inhibition hypothesis, at least insofar as it applies to mice.

Spontaneous alpha modulation and behavior

In this study, we investigated how alpha modulation during baseline activity correlated to performance of a whisker-based selective detection task. Consistent with previous results showing that pre-stimulus alpha modulates sensory encoding in human perceptual-decision making (Lou et al., 2014), we found significant deficits in alpha modulation prior to incorrect (miss or false alarm trials) trials compared to correct (hit or correct rejection) trials (**Fig. 6, 7**). While there were neurons that were significantly phase modulated prior to both correct and incorrect trials, most neurons across regions were selectively phase modulated prior to correct trials, with extremely few neurons showing selective phase modulation prior to incorrect trials (**Fig. 7A**). Additionally, across most regional populations of phase-modulated neurons, MI and MSE of the best fit von Mises distributions were significantly higher prior to incorrect trials than prior to correct trials (**Fig. 7B,C**). This increased deviation from both uniform and von Mises distributions resulted from increased randomness in the relationship between spiking and alpha phase as seen in **Figure 6**. Thus, a dysregulation of alpha modulation of spiking activity during spontaneous activity correlated with poor performance on the selective detection task. This may reflect a lapse in attention or engagement in the task.

Similar to many tactile tasks, the behavioral task employed in this study involves the coordinated activity of numerous brain regions, including thalamus, S1, motor cortex, anterior lateral motor cortex, and striatum (Zheng et al., 2015; Delis et al., 2018; Rodenkirch et al., 2019; Aruljothi et al., 2020; Zareian et al., 2021; Marrero et al., 2022; Zareian et al., 2023). Marrero et al. (2022) found that correct responses to sensory stimuli were predicted by a pre-stimulus global low amplitude state across cortex with reduced spontaneous activity, principally identified through widefield calcium imaging of activity in dorsal neocortex. The low activity state associated with correct task performance was most prominent in neurons that encode stimuli or were associated with motor response. This suggests that a quiet brain state is preferable for neural circuits to process information suited for detection tasks, likely at the cost of discrimination performance

(Wang et al., 2010; Ollerenshaw et al., 2014). Based on our observations, this global cortical low amplitude state is, at least in part, a result of the ubiquity of alpha modulation and pulsed inhibition in neocortex. Alpha oscillations have been hypothesized to produce a brain state which is “calm yet alert” (Adrian and Matthews, 1934; Cooper et al., 2003), which is in line with the brain state characterized by the global low amplitude state and strong alpha modulation associated with correct responses on the selective detection task. Furthermore, the propensity of neurons in the low activity state to more strongly represent tactile stimuli is mirrored by our observations that phase-modulated neurons responded more strongly to tactile stimuli (**Fig. 3**).

Buffalo et al. (2011) evaluated the coherence between multi-unit activity and LFPs, which is comparable to phase modulation, in visual cortex of macaques performing a cued visual attention task and found reduced coherence between multi-unit activity and low frequency oscillations (including alpha) while the monkey attended to visual stimuli. At first, this may seem to contradict our observation of weaker alpha modulation prior to incorrect trials; however, in the visual attention task, monkeys were cued to attend to the visual stimulus (requiring internal direction of attention), while the mice performing the tactile selective detection task received no cue prior to stimulus presentation. The tasks were therefore sufficiently distinct that too close a comparison would be inappropriate. The selective detection task employed here does not require the fine discrimination tactile stimuli; instead, it requires all-or-none responses to stimuli distributed across much of the whisker pad. The strong alpha modulation observed prior to correct trials compared to incorrect trials, rather than reflecting the sort of internally directed attention described in Buffalo et al. (2011), instead may produce the global low amplitude activity, identified by Marrero et al. (2022), which tunes brain networks to the discrete all-or-none behavior required for this task (Hô and Destexhe, 2000).

A number of studies have associated disruptions in phase modulation of spiking activity in pathological and pharmacologically altered brain states (Sigurdsson et al., 2010; Lopez-Pigozzi et al., 2016; Lazaro et al., 2019; Golden and Chadderton, 2022; Weiss et al., 2023). Golden and Chadderton (2022) injected mice with psilocybin and observed reduced coupling of single-unit spiking activity to different LFP bands (delta, theta, alpha and beta) in anterior cingulate cortex. While that study focused on the effects of psilocybin on the physiology of anterior cingulate rather than mouse behavior, it is interesting to note that attention deficits associated with psilocybin more likely reflect a decreased ability to suppress and ignore distraction than a reduction in attentional capacity per se (Carter et al., 2005), and alpha oscillations are strongly implicated in the suppression of distractors (Cooper et al., 2003; Klimesch et al., 2007; Palva and Palva, 2007; Lazaro et al., 2019). Lazaro et al. (2019) observed alterations in phase modulation in PFC of a mouse model of autism (CNTNAP2 KO). While they did not link altered phase modulation, or disruption of network dynamics more generally, to specific behavioral differences, it is noteworthy that autism is associated with cognitive and attentional deficits (Cantio et al., 2016; Muskens et al., 2017). Taken together, these studies suggest that alpha modulation is a feature of a properly functioning cortex and subject to pathological and pharmacological dysfunction. A recent study developed a real-time system for stimulating neural populations at particular phases of LFP oscillations (Wick et al., 2023). Future work may harness such techniques to investigate whether

cognitive performance can be improved by stimulating cortical neurons at appropriate phases of the alpha rhythm during spontaneous activity.

Acknowledgements

This work was supported by AFOSR FA9550-22–1-0337, NSF CBET 1847315, NIH R01NS119813, and NIH R01AG075114.

Disclaimer

Q.W. is the co-founder of Sharper Sense.

Figures

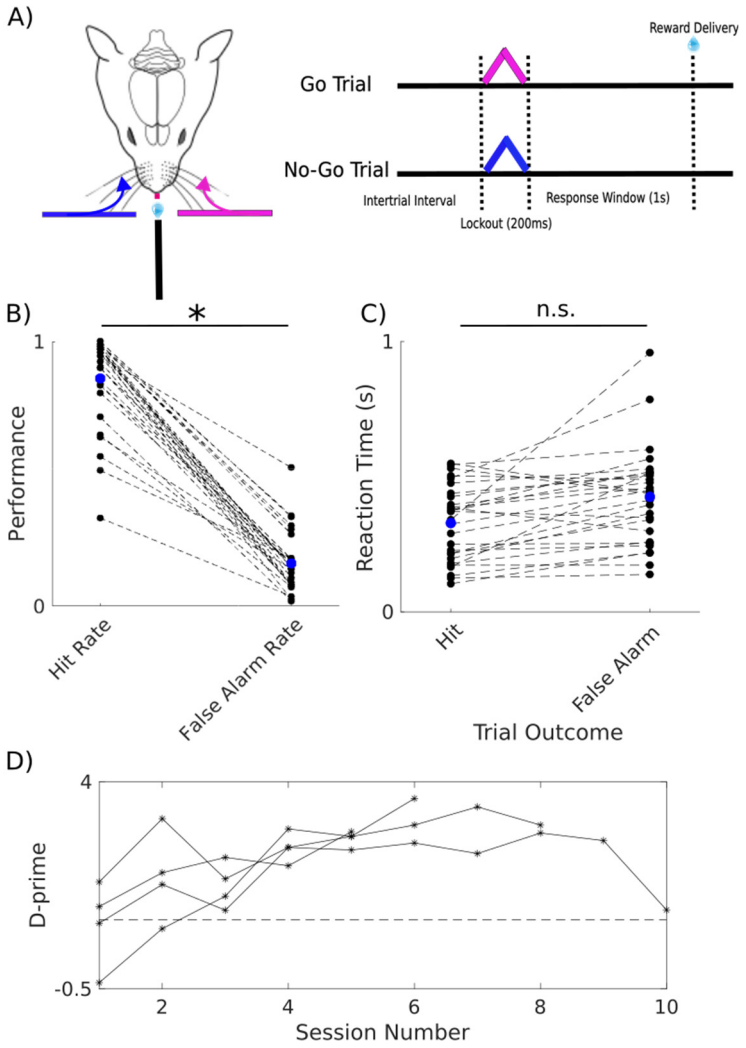

Figure 1. Behavioral task and performance. ***(A)*** *Schematic representation of a whisker-based selective detection task. Head-fixed mice were required to lick a waterspout during a 1 s response window following left-sided whisker deflections (go stimuli) to receive a water reward. They were required to withhold licks in response to right-sided deflections (no-go stimuli) during the window of opportunity to avoid a longer inter-trial interval.* ***(B)*** *Expert mice exhibited significantly higher hit rates than false alarm rates. Average hit and false alarm rates shown in blue.* ***(C)*** *Reaction times did not differ significantly between hits and false alarms. Data from individual sessions are connected by dashed lines. Average reaction times shown in blue.* ***(D)*** *Discriminability across sessions for each mouse. d' = 1 shown with dashed line.*

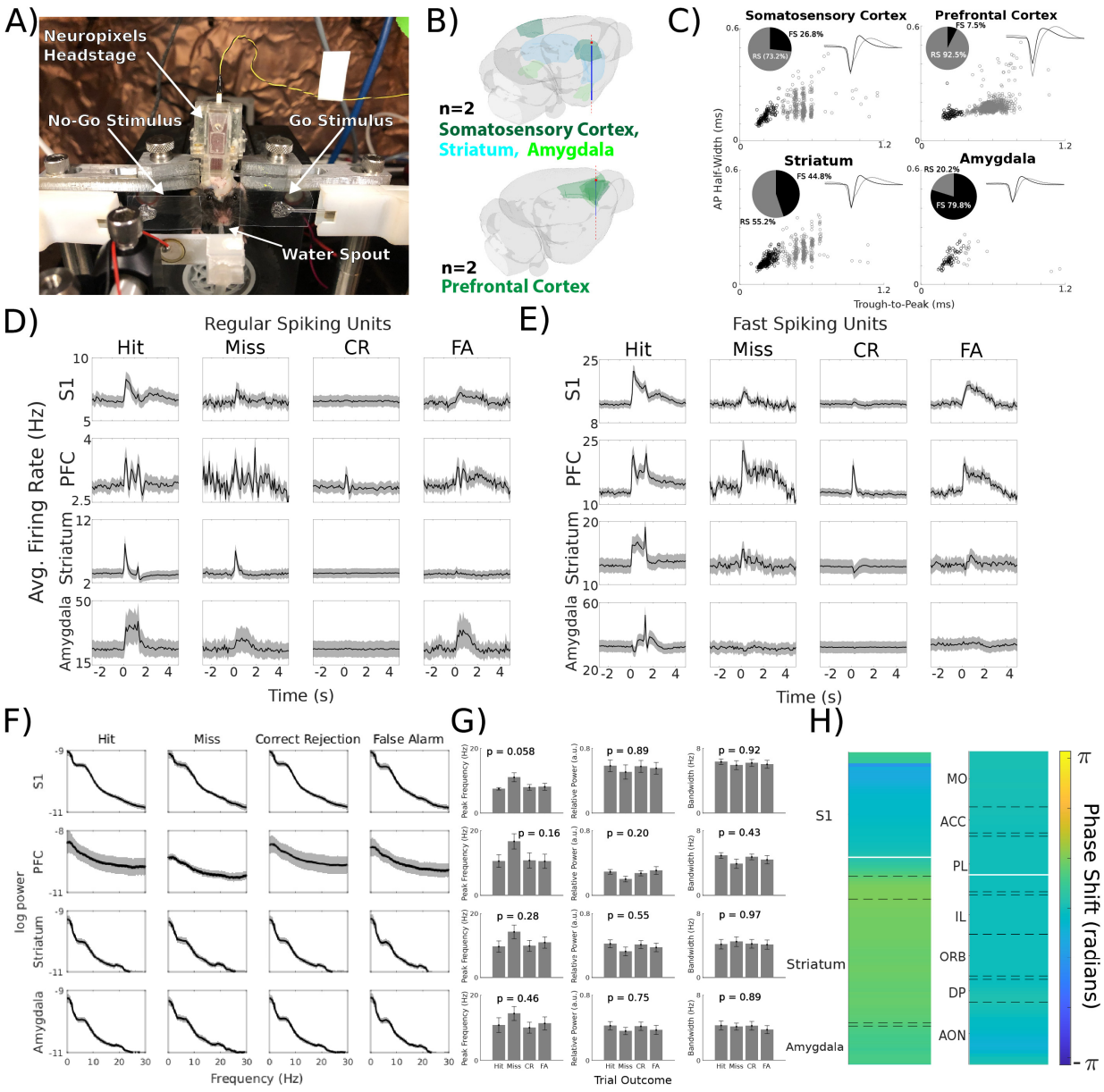

Figure 2: Neural activity across different brain regions during the tactile selective detection task. ***(A)*** *Photo of head-fixed mouse with chronically implanted Neuropixels 1.0 electrode in S1, striatum, and amygdala performing the whisker-based selective detection task.* ***(B)*** *3D renderings of probe trajectories planned with Neuropixels Trajectory Explorer.* ***(C)*** *Classification of RS and FS units in S1, PFC, striatum, and amygdala based on the time from the trough of the waveform to the subsequent peak and the width of the negative deflection.* ***(D)*** *Average firing rates of all RS units in S1 (n = 325), PFC (n = 769), striatum (n = 334) and amygdala (n = 17) separated by trial outcome and aligned to the tactile stimulus.* ***(E)*** *Average firing rates of all FS units in S1 (n = 120), PFC (n = 50, center), striatum (n = 271), and amygdala (n = 66) separated by trial outcome and aligned to the tactile stimulus.* ***(F)*** *Average LFP spectra separated by trial outcome across all sessions from electrodes in S1 (layer 5), PFC (PL), striatum (caudoputamen), and amygdala (lateral amygdala).* ***(G)*** *Summary of periodic components (local peak center frequencies, relative power, and bandwidth) of LFP spectra used to compute averages shown in* ***(F)****.* ***(H)*** *Average alpha-band phase shift across brain regions relative to reference electrodes (represented with white lines; left: S1 layer 5; right: PL).*

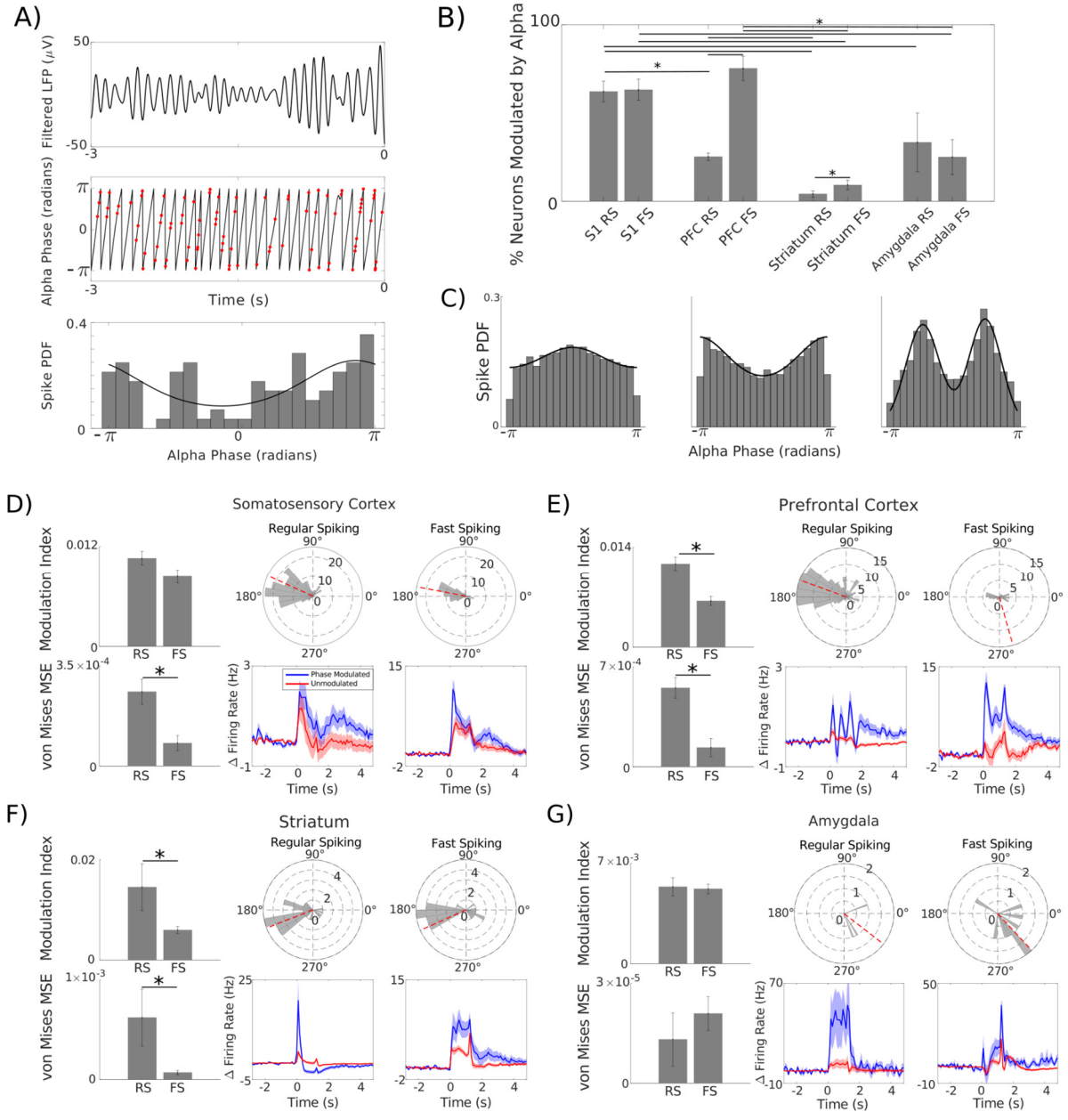

Figure 3: Alpha phase modulation of single-unit activity across different brain regions. ***(A)*** *Example of phase modulation of spiking activity during baseline activity on a single trial. (Top) 3 s alpha band (8 - 12 Hz) filtered LFP. (Center) Instantaneous phase of filtered LFP computed via Hilbert transform (black). Spike times from a single neuron recorded on the same electrode are overlaid in red. (Bottom) Spiking probability density at binned phases of alpha. The best fit von Mises distribution is overlaid in black.* ***(B)*** *Percentages of RS and FS units which were significantly alpha phase-modulated across brain regions.* ***(C)*** *Examples of spike distributions across alpha phase. Left and center are best characterized by a von Mises distribution (circular analog of a normal distribution); right is better characterized by a bimodal distribution.* ***(D-G)*** *Averages of MI, MSE of the best fit von Mises distribution, and preferred alpha phase of spiking for phase-modulated RS and FS units, as well as comparisons of average baseline normalized firing rates for phase-modulated and non-phase-modulated units, across brain regions.*

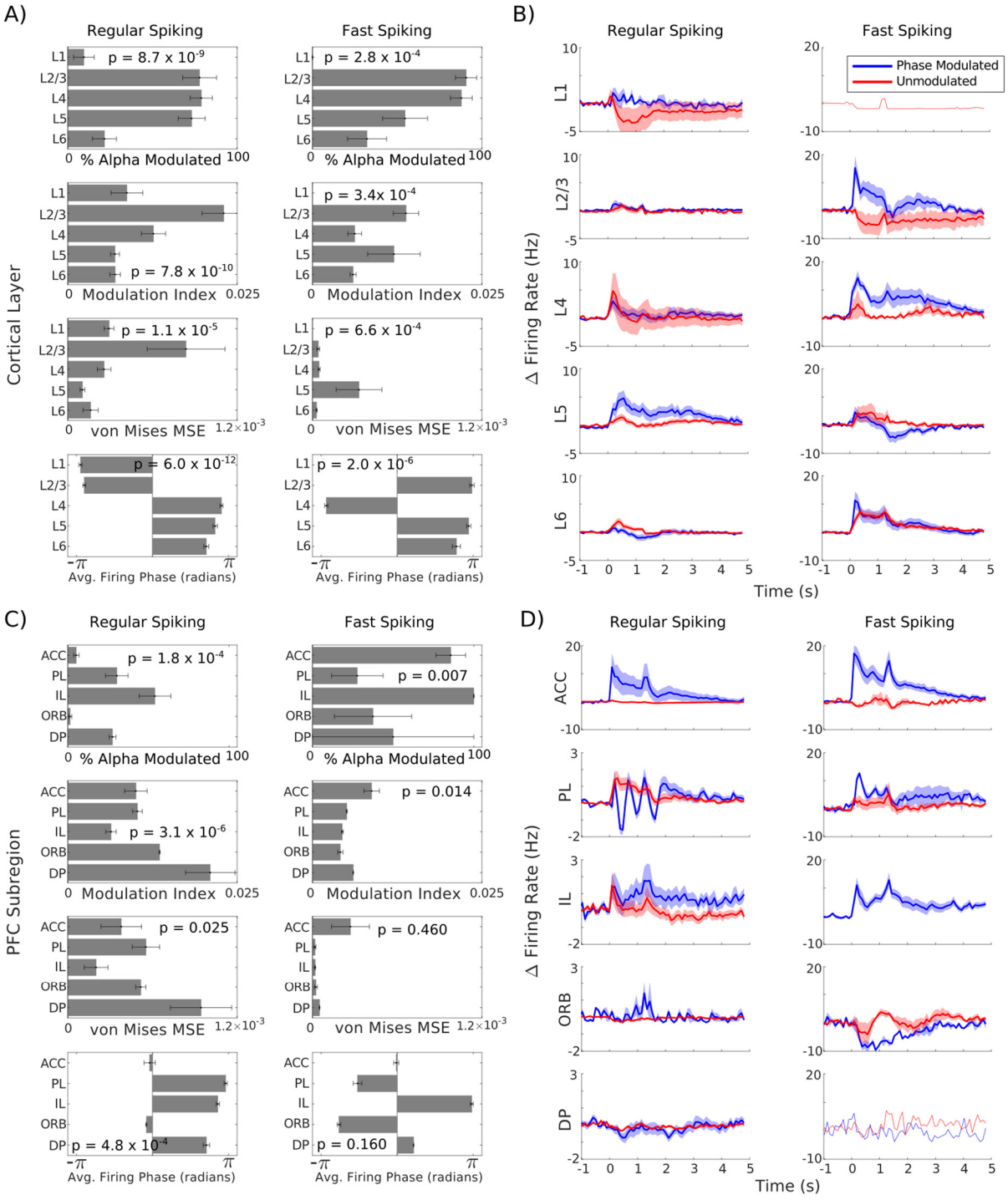

Figure 4. Phase modulation varies across cortical layers in S1 and PFC subregions. *(Top to bottom) Percent of RS (left) and FS (units) that were phase modulated, MI, MSE of best fit von Mises distributions, and average firing phase in different (**A**) S1 cortical layers and (**C**) PFC subregions. Comparisons of average baseline normalized firing rates between phase modulated (blue) and non-phase modulated (red) units in each (**B**) S1 cortical layer and (**D**) PFC subregion.*

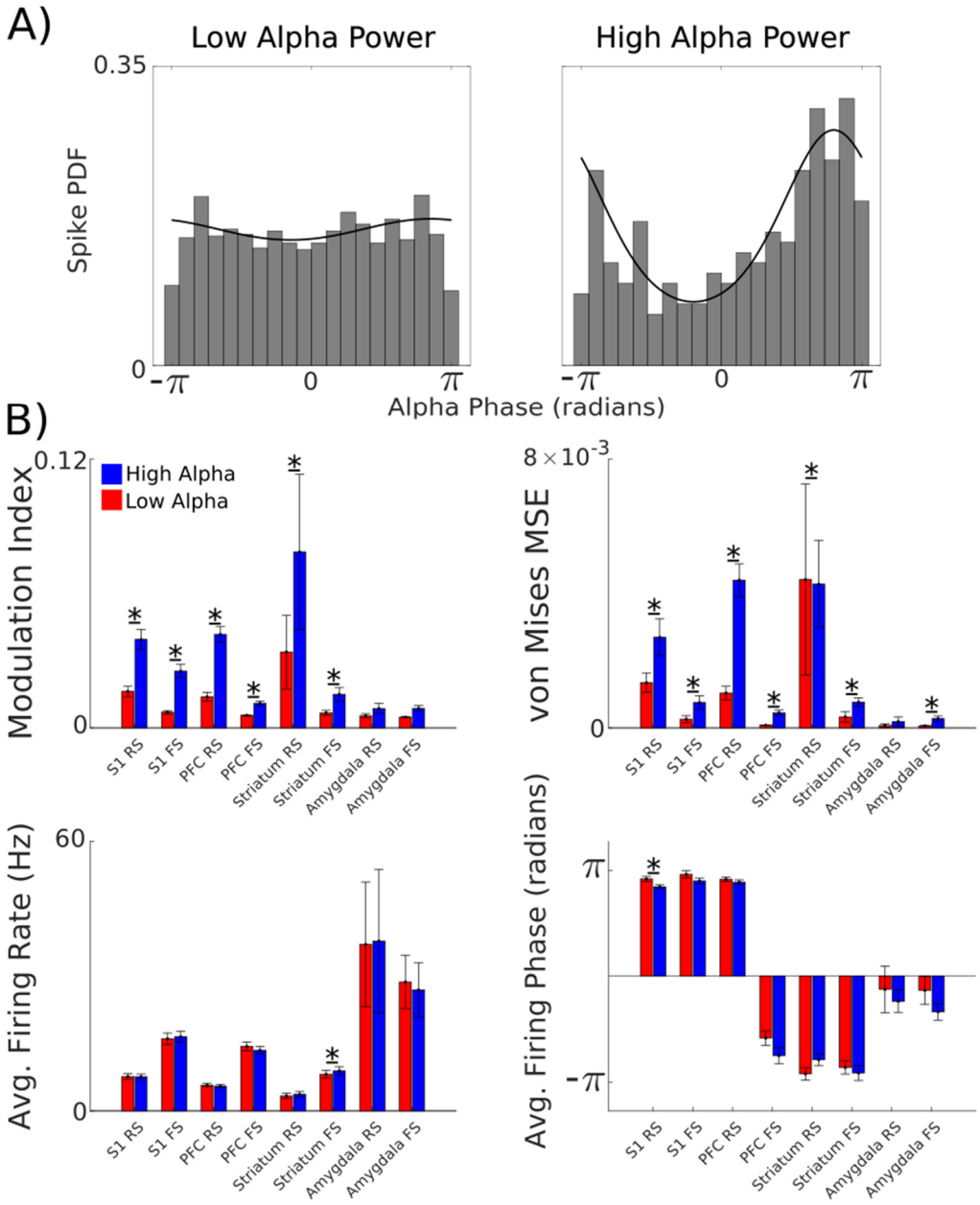

Figure 5: Phase modulation of single-unit activity changes with alpha power. (A) *Example of spike distributions across alpha phase during low alpha power events (left, ≥ 0.3 s when alpha power is below its 50th percentile) and high alpha power events (right, 0.3 s when alpha power is above its 75th percentile).* ***(B)*** *Average MI, MSE of the best fist von Mises distribution, firing rate, and preferred alpha phase across spikes during low (red) and high (blue) alpha power events.*

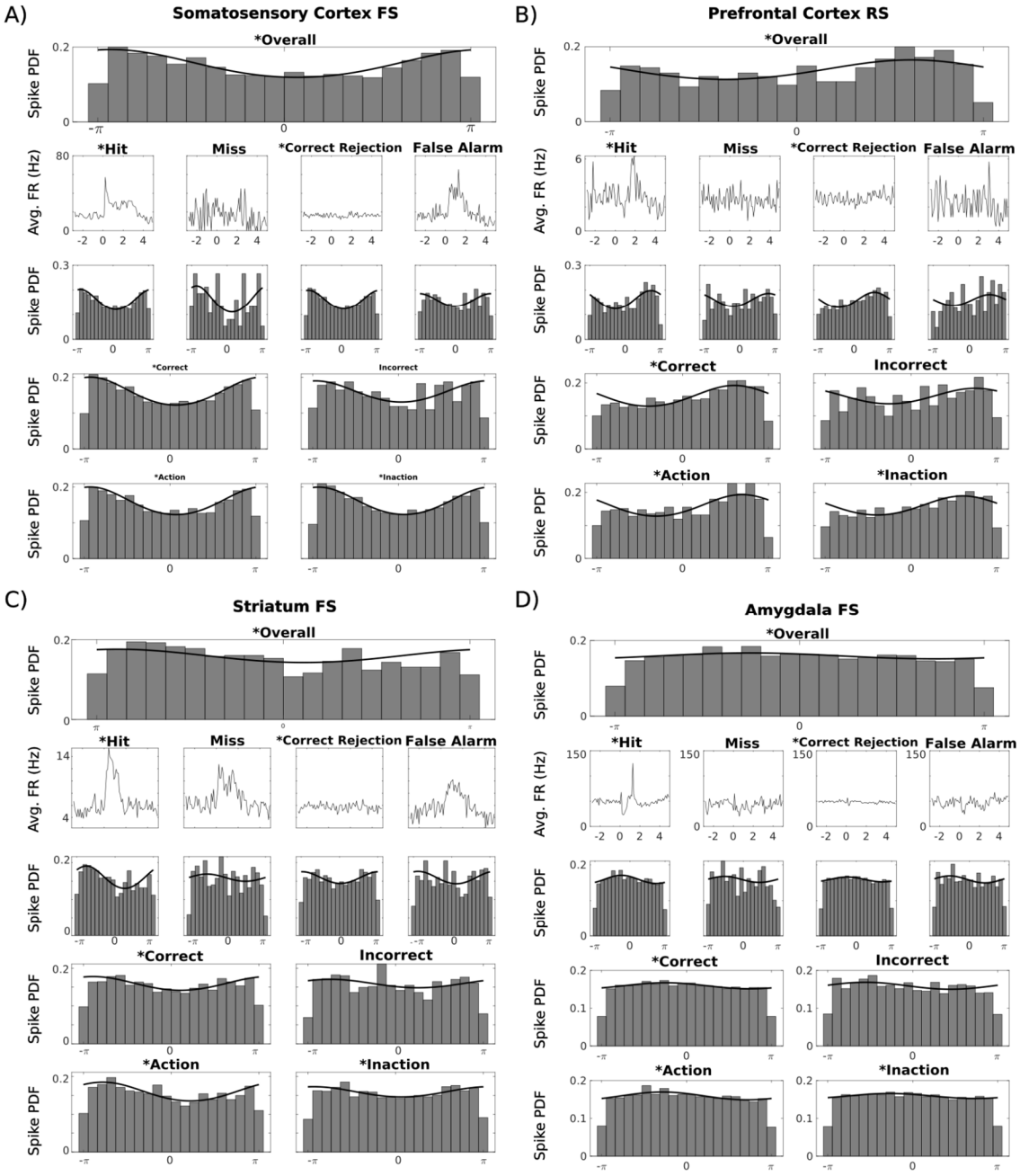

Figure 6: Baseline alpha phase modulation correlates with behavior in single neurons. *Examples of phase-modulated neurons in (**A**) S1, (**B**) PFC, (**C**) striatum, and (**D**) amygdala. * indicates significant phase modulation. On the top row, all baseline spikes (3 s prior to stimulus) are pooled together regardless of trial outcome. On the next row are average firing rates for that neuron for each trial outcome. Below are spike probability distributions for baseline spikes pooled across all trials of the above outcome. On the next row, spike probability distributions were generated based on cognitive outcomes: correct and incorrect. In the final row, spike probability distributions were generated based on motor outcomes: action and inaction.*

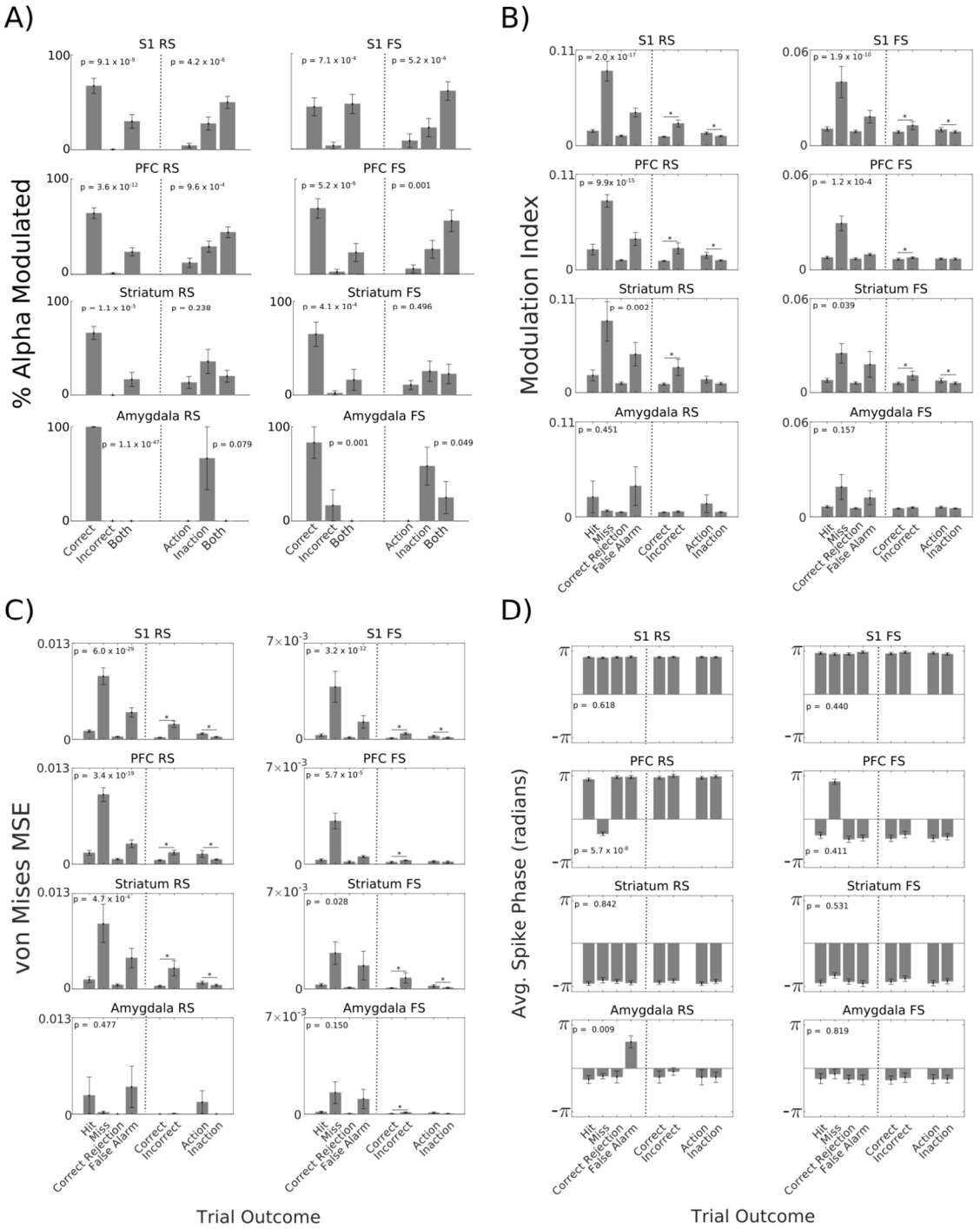

Figure 7: Incorrect trials were preceded by a disruption in alpha phase modulation. ***(A)*** *Right: Percentages of neurons which were selectively phase modulated prior to correct trials, selectively phase modulated prior to incorrect trials, and phase modulated regardless of cognitive outcome. Left: Percentages of neurons which were selectively phase modulated prior to action trials, selectively phase modulated prior to inaction trials, and phase modulated regardless of motor outcome.* ***(B)*** *MI of best fit von Mises distributions for each behavioral outcome.* ***(C)*** *MSE of best fit von Mises distributions for each behavioral outcome.* ***(D)*** *Preferred alpha phase of spiking separated by behavioral outcomes.*

References

Adrian ED, Matthews BHC (1934) The Berger rhythm: potential changes from the occipital lobes in man. Brain: A Journal of Neurology 57:355-385.

Agmon A, Connors BW (1992) Correlation between intrinsic firing patterns and thalamocortical synaptic responses of neurons in mouse barrel cortex. J Neurosci 12:319-329.

Aruljothi K, Marrero K, Zhang Z, Zareian B, Zagha E (2020) Functional Localization of an Attenuating Filter within Cortex for a Selective Detection Task in Mice. The Journal of Neuroscience 40:5443.

Bagherzadeh Y, Baldauf D, Pantazis D, Desimone R (2020) Alpha Synchrony and the Neurofeedback Control of Spatial Attention. Neuron 105:577-587.e575.

Berger H (1929) Über das Elektrenkephalogramm des Menschen. Archiv für Psychiatrie und Nervenkrankheiten 87:527-570.

Bollimunta A, Chen Y, Schroeder CE, Ding M (2008) Neuronal mechanisms of cortical alpha oscillations in awake-behaving macaques. J Neurosci 28:9976-9988.

Bollimunta A, Mo J, Schroeder CE, Ding M (2011) Neuronal mechanisms and attentional modulation of corticothalamic α oscillations. J Neurosci 31:4935-4943.

Buffalo EA, Fries P, Landman R, Buschman TJ, Desimone R (2011) Laminar differences in gamma and alpha coherence in the ventral stream. Proc Natl Acad Sci U S A 108:11262-11267.

Buzsáki G, Draguhn A (2004) Neuronal Oscillations in Cortical Networks. Science 304:1926-1929.

Cantio C, Jepsen JR, Madsen GF, Bilenberg N, White SJ (2016) Exploring 'The autisms' at a cognitive level. Autism Res 9:1328-1339.

Carter OL, Burr DC, Pettigrew JD, Wallis GM, Hasler F, Vollenweider FX (2005) Using psilocybin to investigate the relationship between attention, working memory, and the serotonin 1A and 2A receptors. Journal of cognitive neuroscience 17:1497-1508.

Castro-Alamancos MA, Tawara-Hirata Y (2007) Area-specific resonance of excitatory networks in neocortex: control by outward currents. Epilepsia 48:1572-1584.

Cooper NR, Croft RJ, Dominey SJ, Burgess AP, Gruzelier JH (2003) Paradox lost? Exploring the role of alpha oscillations during externally vs. internally directed attention and the implications for idling and inhibition hypotheses. Int J Psychophysiol 47:65-74.

da Silva FH, van Lierop TH, Schrijer CF, van Leeuwen WS (1973) Essential differences between alpha rhythms and barbiturate spindles: spectra and thalamo-cortical coherences. Electroencephalogr Clin Neurophysiol 35:641-645.

Dahl MJ, Ilg L, Li SC, Passow S, Werkle-Bergner M (2019) Diminished pre-stimulus alpha-lateralization suggests compromised self-initiated attentional control of auditory processing in old age. Neuroimage 197:414-424.

Davis ZW, Dotson NM, Franken TP, Muller L, Reynolds JH (2023) Spike-phase coupling patterns reveal laminar identity in primate cortex. Elife 12.

Delis I, Dmochowski JP, Sajda P, Wang Q (2018) Correlation of neural activity with behavioral kinematics reveals distinct sensory encoding and evidence accumulation processes during active tactile sensing. NeuroImage 175:12-21.

Donoghue T, Haller M, Peterson EJ, Varma P, Sebastian P, Gao R, Noto T, Lara AH, Wallis JD, Knight RT, Shestyuk A, Voytek B (2020) Parameterizing neural power spectra into periodic and aperiodic components. Nature Neuroscience 23:1655-1665.

Dougherty K, Cox MA, Ninomiya T, Leopold DA, Maier A (2017) Ongoing Alpha Activity in V1 Regulates Visually Driven Spiking Responses. Cereb Cortex 27:1113-1124.

Eschenko O, Magri C, Panzeri S, Sara SJ (2012) Noradrenergic neurons of the locus coeruleus are phase locked to cortical up-down states during sleep. Cereb Cortex 22:426-435.

Fisher NI (1993) Statistical Analysis of Circular Data. Cambridge: Cambridge University Press.

Gage GJ, Stoetzner CR, Wiltschko AB, Berke JD (2010) Selective activation of striatal fast-spiking interneurons during choice execution. Neuron 67:466-479.

Golden CT, Chadderton P (2022) Psilocybin reduces low frequency oscillatory power and neuronal phase-locking in the anterior cingulate cortex of awake rodents. Sci Rep 12:12702.

Gray CM, Konig P, Engel AK, Singer W (1989) Oscillatory responses in cat visual cortex exhibit inter-columnar synchronization which reflects global stimulus properties. Nature 338:334-337.

Haegens S, Nácher V, Luna R, Romo R, Jensen O (2011) α-Oscillations in the monkey sensorimotor network influence discrimination performance by rhythmical inhibition of neuronal spiking. Proc Natl Acad Sci U S A 108:19377-19382.

Händel BF, Haarmeier T, Jensen O (2011) Alpha oscillations correlate with the successful inhibition of unattended stimuli. Journal of cognitive neuroscience 23:2494-2502.

Hô N, Destexhe A (2000) Synaptic background activity enhances the responsiveness of neocortical pyramidal neurons. J Neurophysiol 84:1488-1496.

Hocker DL, Brody CD, Savin C, Constantinople CM (2021) Subpopulations of neurons in lOFC encode previous and current rewards at time of choice. eLife 10:e70129.

Jensen O, Mazaheri A (2010) Shaping functional architecture by oscillatory alpha activity: gating by inhibition. Front Hum Neurosci 4:186.

Jones SR, Pinto DJ, Kaper TJ, Kopell N (2000) Alpha-frequency rhythms desynchronize over long cortical distances: a modeling study. J Comput Neurosci 9:271-291.

Jung YJ, Sun SH, Almasi A, Yunzab M, Meffin H, Ibbotson MR (2023) Characterization of extracellular spike waveforms recorded in wallaby primary visual cortex. Front Neurosci 17:1244952.

Klimesch W, Sauseng P, Hanslmayr S (2007) EEG alpha oscillations: the inhibition-timing hypothesis. Brain Res Rev 53:63-88.

Lakatos P, Shah AS, Knuth KH, Ulbert I, Karmos G, Schroeder CE (2005) An oscillatory hierarchy controlling neuronal excitability and stimulus processing in the auditory cortex. J Neurophysiol 94:1904-1911.

Lazaro MT et al. (2019) Reduced Prefrontal Synaptic Connectivity and Disturbed Oscillatory Population Dynamics in the CNTNAP2 Model of Autism. Cell reports 27:2567-2578.e2566.

Lehtelä L, Salmelin R, Hari R (1997) Evidence for reactive magnetic 10-Hz rhythm in the human auditory cortex. Neurosci Lett 222:111-114.

Liu YA, Nong Y, Feng J, Li G, Sajda P, Li Y, Wang Q (2024) Phase synchrony between prefrontal noradrenergic and cholinergic signals indexes inhibitory control. bioRxiv.

Lopez-Pigozzi D, Laurent F, Brotons-Mas JR, Valderrama M, Valero M, Fernandez-Lamo I, Cid E, Gomez-Dominguez D, Gal B, Menendez de la Prida L (2016) Altered Oscillatory Dynamics of CA1 Parvalbumin Basket Cells during Theta-Gamma Rhythmopathies of Temporal Lobe Epilepsy. eNeuro 3.

Lou B, Li Y, Philiastides MG, Sajda P (2014) Prestimulus alpha power predicts fidelity of sensory encoding in perceptual decision making. Neuroimage 87:242-251.

Lukatch HS, MacIver MB (1997) Physiology, pharmacology, and topography of cholinergic neocortical oscillations in vitro. J Neurophysiol 77:2427-2445.

Marrero K, Aruljothi K, Zareian B, Gao C, Zhang Z, Zagha E (2022) Global, Low-Amplitude Cortical State Predicts Response Outcomes in a Selective Detection Task in Mice. Cereb Cortex 32:2037-2053.

Mathewson KE, Lleras A, Beck DM, Fabiani M, Ro T, Gratton G (2011) Pulsed out of awareness: EEG alpha oscillations represent a pulsed-inhibition of ongoing cortical processing. Front Psychol 2:99.

Mazaheri A, Jensen O (2010) Rhythmic pulsing: linking ongoing brain activity with evoked responses. Front Hum Neurosci 4:177.
Mitra P, Bokil H (2007) Observed Brain Dynamics. In: Oxford University Press.
Muskens JB, Velders FP, Staal WG (2017) Medical comorbidities in children and adolescents with autism spectrum disorders and attention deficit hyperactivity disorders: a systematic review. Eur Child Adolesc Psychiatry 26:1093-1103.
Ojha P (2024) Berger and the Breakthrough: A Centennial Celebration of the Human Electroencephalogram. Neurodiagn J 64:69-74.
Ollerenshaw Douglas R, Zheng He JV, Millard Daniel C, Wang Q, Stanley Garrett B (2014) The adaptive trade-off between detection and discrimination in cortical representations and behavior. Neuron 81:1152-1164.
Pachitariu M, Sridhar S, Pennington J, Stringer C (2024) Spike sorting with Kilosort4. Nature methods 21:914-921.
Palva S, Palva JM (2007) New vistas for alpha-frequency band oscillations. Trends Neurosci 30:150-158.
Riedemann T (2019) Diversity and Function of Somatostatin-Expressing Interneurons in the Cerebral Cortex. Int J Mol Sci 20.
Rodenkirch C, Liu Y, Schriver BJ, Wang Q (2019) Locus coeruleus activation enhances thalamic feature selectivity via norepinephrine regulation of intrathalamic circuit dynamics. Nature Neuroscience 22:120-133.
Rosenkranz JA, Grace AA (1999) Modulation of basolateral amygdala neuronal firing and afferent drive by dopamine receptor activation in vivo. J Neurosci 19:11027-11039.
Schneider D, Göddertz A, Haase H, Hickey C, Wascher E (2019) Hemispheric asymmetries in EEG alpha oscillations indicate active inhibition during attentional orienting within working memory. Behav Brain Res 359:38-46.
Sigurdsson T, Stark KL, Karayiorgou M, Gogos JA, Gordon JA (2010) Impaired hippocampal-prefrontal synchrony in a genetic mouse model of schizophrenia. Nature 464:763-767.
Someck S, Levi A, Sloin HE, Spivak L, Gattegno R, Stark E (2023) Positive and biphasic extracellular waveforms correspond to return currents and axonal spikes. Commun Biol 6:950.
Stanislaw H, Todorov N (1999) Calculation of signal detection theory measures. Behavior Research Methods, Instruments, & Computers 31:137-149.
Steriade M, Gloor P, Llinás RR, Lopes de Silva FH, Mesulam MM (1990) Report of IFCN Committee on Basic Mechanisms. Basic mechanisms of cerebral rhythmic activities. Electroencephalogr Clin Neurophysiol 76:481-508.
Tort AB, Komorowski R, Eichenbaum H, Kopell N (2010) Measuring phase-amplitude coupling between neuronal oscillations of different frequencies. J Neurophysiol 104:1195-1210.
van Kerkoerle T, Self MW, Dagnino B, Gariel-Mathis MA, Poort J, van der Togt C, Roelfsema PR (2014) Alpha and gamma oscillations characterize feedback and feedforward processing in monkey visual cortex. Proc Natl Acad Sci U S A 111:14332-14341.
VanRullen R, Koch C (2003) Is perception discrete or continuous? Trends Cogn Sci 7:207-213.
Wang Q, Webber R, Stanley GB (2010) Thalamic Synchrony and the Adaptive Gating of Information Flow to Cortex. Nature Neuroscience 13:1534-1541.
Weiss E, Kann M, Wang Q (2023) Neuromodulation of Neural Oscillations in Health and Disease. Biology 12.
Wick ZC, Philipsberg PA, Lamsifer SI, Kohler C, Katanov E, Feng Y, Humphrey C, Shuman T (2023) Manipulating single-unit theta phase-locking with PhaSER: An open-source tool for real-time phase estimation and manipulation. bioRxiv.
Wildegger T, van Ede F, Woolrich M, Gillebert CR, Nobre AC (2017) Preparatory α-band oscillations reflect spatial gating independently of predictions regarding target identity. J Neurophysiol 117:1385-1394.

Worden MS, Foxe JJ, Wang N, Simpson GV (2000) Anticipatory biasing of visuospatial attention indexed by retinotopically specific alpha-band electroencephalography increases over occipital cortex. J Neurosci 20:Rc63.

Xu X, Roby KD, Callaway EM (2010) Immunochemical characterization of inhibitory mouse cortical neurons: three chemically distinct classes of inhibitory cells. J Comp Neurol 518:389-404.

Yamada H, Inokawa H, Hori Y, Pan X, Matsuzaki R, Nakamura K, Samejima K, Shidara M, Kimura M, Sakagami M, Minamimoto T (2016) Characteristics of fast-spiking neurons in the striatum of behaving monkeys. Neurosci Res 105:2-18.

Zareian B, Zhang Z, Zagha E (2021) Cortical Localization of the Sensory-Motor Transformation in a Whisker Detection Task in Mice. eNeuro 8.

Zareian B, Lam A, Zagha E (2023) Dorsolateral Striatum is a Bottleneck for Responding to Task-Relevant Stimuli in a Learned Whisker Detection Task in Mice. J Neurosci 43:2126-2139.

Zheng HJV, Wang Q, Stanley GB (2015) Adaptive shaping of cortical response selectivity in the vibrissa pathway. Journal of Neurophysiology 113:3850-3865.